Probing the Nature of Strain-Induced Crystallization in Polyisoprene Rubber by Combined Thermomechanical and In Situ X-ray Diffraction Techniques

Shigeyuki Toki,*,† Igors Sics,† Benjamin S. Hsiao,*,† Masatoshi Tosaka,‡ Sirilux Poompradub,‡ Yuko Ikeda,§ and Shinzo Kohjiya‡

Department of Chemistry, State University of New York at Stony Brook, Stony Brook, New York 11794-3400, Institute for Chemical Research, Kyoto University, Uji, Kyoto-fu 611-0011, Japan, and Department of Chemistry and Materials Technology, Kyoto Institute of Technology, Matsugasaki, Sakyo-ku, Kyoto 606-8585, Japan

Received March 5, 2005; Revised Manuscript Received May 8, 2005

ABSTRACT: The nature of strain-induced crystallization in vulcanized polyisoprene rubbers was investigated by in situ synchrotron wide-angle X-ray diffraction under varying thermomechanical conditions. In particular, the methods of constrained cooling and constrained heating under constant strain were used to explore the relationships between the strain-induced crystalline network and corresponding stress. It was found that constrained cooling resulted in a large reduction of stress and a notable increase in the amount of strain-induced crystallites, while constrained heating led to an initial increase in stress and subsequent melting of strain-induced crystallites. Results indicate that strain-induced crystallization induces a new network structure, which reinforces the chemical network points. However, the sulfur bridges in the chemical network points would break down at high temperatures under high strains, despite the existence of strain-induced crystalline network.

Introduction

The relationships between stress- and strain-induced crystallization in nature and synthetic rubbers during uniaxial tensile deformation have been extensively studied in theories and by experiments since the 1940s.[1−15] In theoretical development, there are two main schools of thought to explain the stress "upturn" at high strains: one is based on the concept of strain-induced crystallization,[1−4] and one is based on the concept of limited extensibility using non-Gaussian chain models.[5−8] In experimental studies, there have been many in situ and ex situ studies demonstrated, with wide-angle X-ray diffraction (WAXD) being the primary technique to probe the relationships among structure, crystallinity, and strain.[8−13]

Recently, the use of synchrotron WAXD in combination with the stretching technique has allowed us to directly "visualize" the structure and stress−strain relations during deformation of rubbers in real time.[16−25] New methods for the analysis of WAXD data have further enabled us to extract additional structural information (i.e., fractions of oriented crystal, unoriented crystal, oriented amorphous, and unoriented amorphous phases)[16−19,22−25] besides the conventional data such as unit cell parameters and crystal dimensions. These studies have revealed some new insights into the subject of strain-induced crystallization in rubber, which can be summarized as follows.

1. Strain-induced crystallization is a common phenomenon in rubber materials, including natural rubber (NR), synthetic polyisoprene (IR), polybutadiene (BR), and isoprene−isobutylene rubber (IIR or butyl rubber). The only exception is styrene−butadiene rubber (SBR), which does not crystallize under deformation.[15−23]

2. Strain-induced crystallites always appear in the form of oriented crystals with the chain axis aligned parallel to the stretching direction.[16,17]

3. The fraction of unoriented amorphous chains remains unexpectedly high (more than 50 wt % of the whole molecule) even at very large strains (>500%), which is due to the heterogeneity of the cross-link distribution.[16−18,23]

4. The initial occurrence of strain-induced crystallization decreases the stress, which results in a "downturn" prior to a typical "upturn" in the stress curve. The unique stress behavior can be attributed to the competition between the stress increase by stretching and the stress decrease by strain-induced crystallization.[15,18,23−27] The phenomenon is more significant in synthetic IR rubber than NR.

5. On the basis of the above observations, a new mechanism of strain-induced crystallization in cross-linked rubber has been proposed.[17,18,23] The mechanism consists of the development of a micelle-like extended-chain crystalline network, connected by stretched non-crystalline tie chains, within the scaffolds of chemical network points.[15,17,18,25] The hybrid topology contains a crystalline network scaffold and a chemical network scaffold, where the combined structures dictate the mechanical performance. However, the exact relationship between the two scaffolds is not yet completely understood, which forms the motivation for this work.

In the current study, we have investigated the dynamic nature of a strain-induced crystalline network structure in IR by means of thermomechanical methods and synchrotron radiation. IR was chosen because of its structural similarity with NR but without having extra impurities such as proteins, fatty acids, conjugated phosphoid-lipids, and gel components (more than 50%

* To whom correspondence should be addressed. E-mail: stoki@mail.chem.sunysb.edu (S.T.); bhsiao@notes.cc.sunysb.edu (B.S.H.). Tel.: 631-632-7793. Fax: 631-632-6518.
† State University of New York at Stony Brook.
‡ Kyoto University.
§ Kyoto Institute of Technology.

10.1021/ma050465f CCC: $30.25
Published on Web 07/15/2005

of the total molecules).[18] The chosen thermomechanical conditions were as follows. After stretching, the sample was subjected to different temperature variations at a constant strain, where the stress and corresponding structure changes could be detected simultaneously. In the past, some similar experiments were carried out, although not in a real-time mode. For example, it was reported that the decrease in temperature under constant strain could lead to the reduction of stress due to the enhanced strain-induced crystallization under a larger degree of supercooling.[3,4,23,26−28] It was also reported that the increase in temperature under constant strain could result in the increases in stress and the melt of strain-induced crystallites.[15,25] The use of synchrotron X-rays made it possible to determine the changes of the strain-induced crystalline network in real time.

It is imperative to point out that the behavior of stress relaxation in rubber during crystallization at low temperatures (−6 to −25 °C) under long annealing times (1−30 h) has been carried out since 1954.[28−30] The purpose of these studies was to understand the crystallization process in rubber under isothermal and equilibrium conditions. In these experiments, the samples were often stretched to a strain of 200−300% at room temperature to prevent the occurrence of strain-induced crystallization. Subsequently, the stretched amorphous samples were annealed at low temperatures (−6 to −25 °C) to crystallize, where stress relaxation and volume change were monitored. It was found that stress and volume started to decrease after several hours, depending on the strain applied and the kind of rubber used, and they continued to decrease for 10−100 hours. As the crystalline nucleation and growth processes occur at low temperatures for a long period of time, this type of experiment is often termed "strain-induced crystallization at low temperature" or "low-temperature-induced crystallization" under constant strain. However, these studies are very different from the current work, where the nature of strain-induced crystallization is probed by the combined thermomechanical and synchrotron WAXD methods.

Experimental Section

The chosen rubber was vulcanized synthetic *cis*-1,4 polyisoprene. The composition of the rubber included: active zinc oxide (1.0 part), stearic acid (2.0 parts), CBS (*N*-cyclohexyl-2-benzothiazole sulfonamide) (1.0 part), and sulfur (1.5 parts) per hundred parts of IR (IR2200, JSR). The curing condition was 140 °C for 25 min, using a procedure similar to the one described previously.[23]

Synchrotron WAXD measurements were carried out at the X27C beamline in the National Synchrotron Light Source (NSLS), Brookhaven National Laboratory (BNL). The wavelength of the X-ray used was 1.371 Å. 2D WAXD patterns were recorded by the MAR-CCD X-ray detector (MAR) for quantitative image analysis. The sample-to-detector distance for WAXD was 112.10 mm. The diffraction angle was calibrated using Al_2O_3 (aluminum oxide) as the standard sample. The typical image acquisition time for each scan was 30 s. All measured WAXD images were corrected for beam fluctuations and sample absorption for data analysis.

A modified Instron tensile machine, allowing the symmetric stretching of the sample, was used for the in situ WAXD study.[17−19,23] The instrument permitted the focused X-ray to illuminate the same sample position during deformation. The chosen deformation rate was 10 mm/min for all stretching experiments. The original length of the sample was 25 mm. As a result, the initial rate of deformation was 0.007 s^{-1}. The stress (σ) was measured as $\sigma = F/(d_0 w_0)$, where F represents the force measured by a load cell, d_0 is the original thickness, and w_0 is the original width. The strain (ϵ), in terms of the deformation ratio, can be defined as $\epsilon = (l - l_0)/l_0$, where l_0 is the original clamp−clamp distance.

The thermal conditions were implemented by a custom-made environmental chamber[17,19,23] attached to the tensile machine. The initial stretching processes were carried out at 30 °C. Under constant strain, the stretched sample was then subjected to a heating rate of 2 °C/min or a cooling rate of −2 °C/min. In situ WAXD patterns and corresponding changes of stress were measured simultaneously during stretching and retraction at 30 °C as well as during temperature increase or decrease under constant strain conditions. The data analysis schemes for WAXD images, which have been detailed elsewhere,[17,18,23] were carried out by a software package (POLAR, Stonybrook Technology and Applied Research in New York).

Results and Discussion

The stress−strain curve (with a maximum strain of 6.0) and selected 2D and 3D WAXD patterns during deformation (at a 10 mm/min rate) of synthetic IR at 30 °C are shown in Figure 1. Each WAXD image was taken at the strain indicated by the arrow. It was seen that stress generally increased with strain; however, the increase exhibited an interesting feature at high strains, i.e., the curve showed a decrease in the rate of stress increase at strain around 4.5 (indicated by a vertical bold arrow in Figure 1). This unique region represents the early stages of strain-induced crystallization, which has been explored further by thermomechanical methods and will be discussed in detail later. Generally speaking, the strain regions below and above the initial strain-induced crystallization region can be described as follows.

2D/3D WAXD patterns exhibited an amorphous halo below strain 3.0, while its intensity distribution shifted slightly toward the equator with increasing strain (e.g., strain 3.0). At strain 4.0, the deformation of the halo pattern became more intense, and several weak but distinct crystalline reflections were seen. These reflections were sharp and highly oriented and appeared in smaller numbers than those in fully crystallized patterns (e.g., at strains 5 and 6). These reflections are caused by the first-formed strain-induced crystallites, which are defective in crystalline ordering or registration but highly oriented with respect to the stretching direction. This finding is consistent with the fringe-micelle crystal model induced by strain during deformation of rubber recently proposed by us.[17−19,23−25] In contrast, at strains above 4.5 (e.g., strains 5.0 and 6.0), the WAXD patterns exhibited well oriented crystalline reflections from a monoclinic unit cell with parameters similar to $a = 1.25$ nm, $b = 0.89$ nm, $c = 0.81$ nm, and $\gamma = 92°$, as previously reported by Bunn.[11] It is interesting to see that, even at strains 5.0 and 6.0, one can observe the persistence of the nonoriented amorphous halo, which is consistent with our previous finding that a substantial amount of amorphous chains remain unstretched at high extension.[17,18,23]

Recently, we have reported results of strain-induced crystallization in IR during extension and retraction at 0 °C.[18,19,23] The initiation of strain-induced crystallization can be identified in the stress−strain curve, where the decrease in the rate of stress increase often appears; the retardation of stress upturn often results in a dip in the rate of stress increase. It is noted that the overall behavior of strain-induced crystallization at 30 °C (Figure 1) is weaker than that at 0 °C.[18,23] For example, the initiation of strain-induced crystallization in IR at

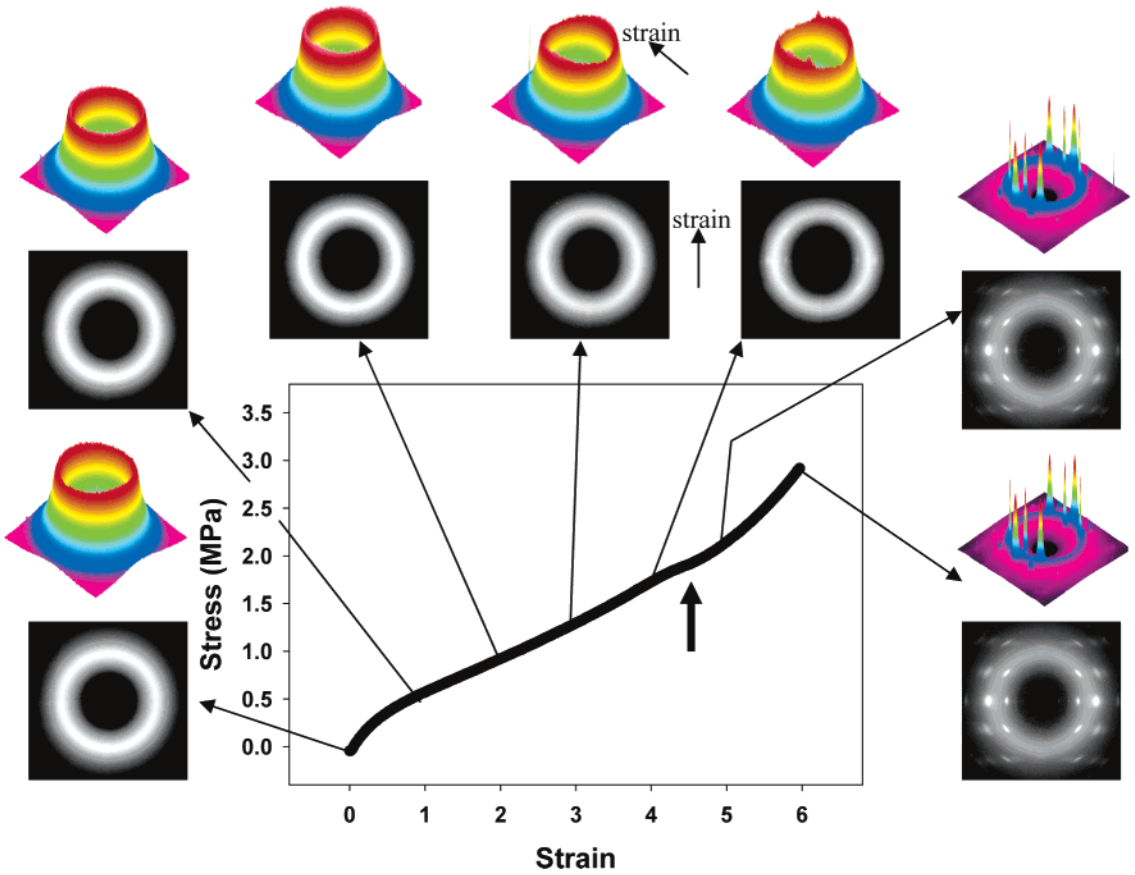

Figure 1. Stress–strain relationship and selected 3D and 2D WAXD patterns collected during stretching of IR at 30 °C. Each image was taken at the average strain indicated by the arrow. The bold vertical arrow shows the onset point in the decrease rate of the stress increase.

0 °C occurs at strain 2.8, while at 30 °C, it occurs at strain 4.5. It is interesting to note that the retardation of the stress upturn in IR is more pronounced than that in NR (although the onset strain for crystallization in NR at 0 °C is 1.8).[17,18,27] The appearance of the stress retardation was found to be a function of deformation rate.[27] The higher strain rate often prolongs the strain-induced crystallization process to higher strains and facilitates the stress-retardation behavior[27] (e.g., a significant stress retardation in IR was reported at a relatively high deformation rate of 0.07 s^{-1} at 29 °C).[26,27] In the following sections, a series of thermomechanical studies in combination with in situ WAXD measurements have been carried out to probe the nature of the strain-induced crystallization, especially at the early stages, and its relationship with the stress response.

1. Stress Relaxation at Constant Strain. Before we describe our results, it is imperative to note that ex situ WAXD studies of strain-induced crystallization in rubber at room temperature have been carried out quite extensively since the 1940s.[9,30] The major deficiency in these studies is that one could not access the effect of time lag between stretching and X-ray measurement, as the rubber sample underwent significant stress relaxation after strain-induced crystallization took place. Some researchers have realized this phenomenon, and they reported that stress relaxation in rubber at room temperature could be followed by monitoring the intensity change of the (120) reflection using a laboratory X-ray source.[14,15] They found that stress relaxation was accompanied by the increase of strain-induced crystallization at room temperature immediately after the cessation of stretching.

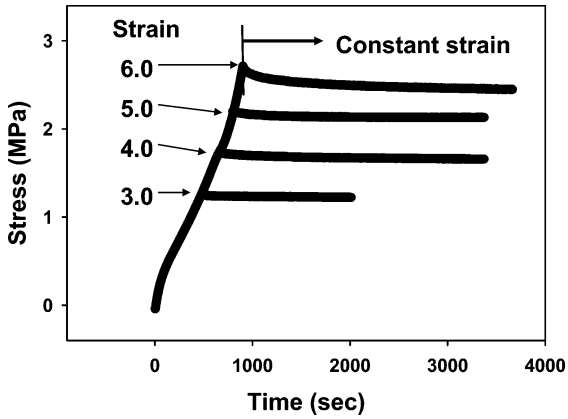

Figure 2. The stress changes during constant rate deformation (the initial rate was 0.007 s^{-1}) at 30 °C and relaxation at constant strains of 3.0, 4.0, 5.0, and 6.0.

In the current work, we have examined this phenomenon in real time at different strains using WAXD with synchrotron radiations. After stretching to a certain strain, the deformed sample was kept at a fixed strain and isothermal condition to examine the stress relaxation behavior with time. Results from the stress relaxation studies at varying strains are shown in Figure 2. It was found that the stress relaxation was most notable at high strains. After stretching to strain 6.0, a large stress decrease was seen. Such decreases became less at strains 4.0 and 5.0. At strain 3.0, the stress decrease was almost negligible.

Figure 3 illustrates the normalized stress relaxation curve (the normalization was carried out by dividing the

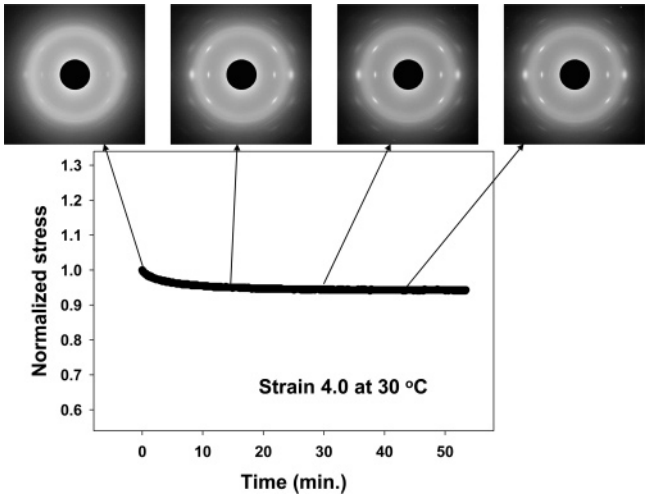

Figure 3. The normalized stress during relaxation process and selected 2D WAXD patterns in IR at 30 °C. Each image was taken at the corresponding time indicated by the arrow.

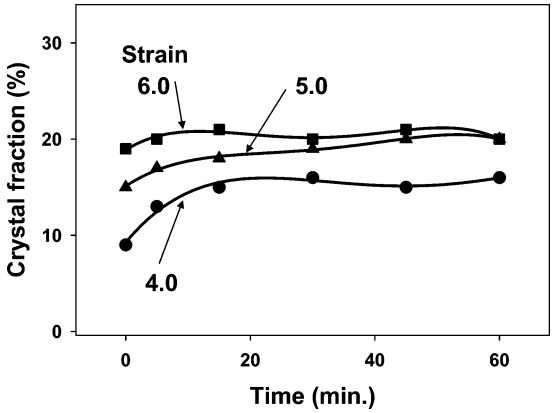

Figure 4. The change of the crystal fraction with time during stress relaxation at strains 4.0, 5.0, and 6.0 for IR at 30 °C.

stress with the maximum value) for the sample stretched to strain 4.0 (i.e., at the early stages of strain-induced crystallization) and selected 2D WAXD patterns at different time intervals. We note that the rate of crystallization at strain 4.0 seems to be much slower than 60 ms, a value previously reported in the literature.[31] The observed WAXD images clearly suggest that crystallization increases with time at the constant strain.

To analyze the WAXD images quantitatively, we have used the following method to evaluate the mass fraction of strain-induced crystallites. The measured 2D flat-plate WAXD image was first transformed into an undistorted geometry in reciprocal space using the procedure described by Fraser et al.[32] The missing data in the meridional region was extrapolated using the expansion of Legendre polynomials

$$I(s,\phi) = \sum a_{2n} P_{2n}(\cos \phi) \tag{1}$$

where $s = 2 \sin(\theta/2)/\lambda$, ϕ represents the azimuthal angle, P_{2n} is the Legendre polynomial of the first kind of order n, and a_{2n} represents the fit coefficient. The fit functions extrapolate into the "missing region", thereby reducing the cutoff error of the integrations. The 2D patterns were integrated cylindrically to determine the intensity profile $I(s)$

$$I(s) = \int I(s,\phi) \sin \phi \, d\phi \tag{2}$$

A peak-fitting procedure was applied to deconvolute the intensity profile into crystalline peaks and an amorphous background using the "Peak Fit" program. The mass fraction of the crystalline phase (or crystal fraction, X_c) was determined as the ratio of the total area under crystalline diffraction peaks to the area under the entire diffraction curve.

Results for the changes of crystal fraction with time at different strains are shown in Figure 4 (the curve at strain 3.0 was not shown, since strain-induced crystallization did not take place at this condition). Two unique features were seen in this figure: (1) the average crystal fraction increased with the increase in applied strain (e.g., the initial values of X_c were 9, 15, and 19% for strains 4, 5, and 6, respectively); (2) at a constant strain, the crystal fraction could increase with time. However, at lower strains, this increase became more pronounced (e.g., the increase of X_c at strain 4.0 was larger than that at strain 5.0). The crystalline fraction at strain 6.0 seemed to become constant with time, despite the fact that the corresponding stress relaxation was the largest (Figure 2).

The above observations can be attributed to the combined effects of (1) the formation of strain-induced crystalline network, which will be discussed further from thermo-mechanical studies, and (2) changes of the chemical network under deformation. We argue that, at strain 3.0, the material behaves like a typical cross-linked elastic material containing only amorphous chains, where the network points are strong enough to bear the stress. At strains 4.0−5.0, strain-induced crystallization takes place. Although the change of crystal fraction seems to be relatively small, the reduction of crystallite size and the rearrangement of crystalline network topology would occur at high strains, resulting in significant stress relaxation. On the other hand, the chemical network points, composed of monosulfur, disulfur, and multisulfur bridges in vulcanized IR can also be rearranged (i.e., the transformations of sulfur bridges from the multisulfur form to the mono- or disulfur forms may occur[33,34]) at very high strains. In particular, at strains closer to the break point (e.g., strain > 6), the readjustment of the chemical network becomes very pronounced, resulting in a large decrease in stress, even though a stable crystalline network has already been formed with relatively high crystallinity (20%). Therefore, the mechanism of stress relaxation should vary with strain; stress relaxation is typically dominated by strain-induced crystallization at high strains. However at strains near the break point, it is dominated by the transformation of chemical network points. The nature of the strain-induced crystallization and its relationship in stress has been explored with the following experiments.

2. Stress Decrease during Constrained Cooling. After stretching to a certain strain at 30 °C, the sample was kept at constant strain and subjected to a cooling sweep at a rate of −2 °C/min (we termed this "constrained cooling"). Results from this experiment are shown in Figure 5, where the stress decrease is seen at all strains. At strains 4.0, 5.0, and 6.0, the stress decreased almost linearly with time (or with decreasing temperature), with the rate of the stress decrease being the fastest at strain 6.0. The stress decrease at strain

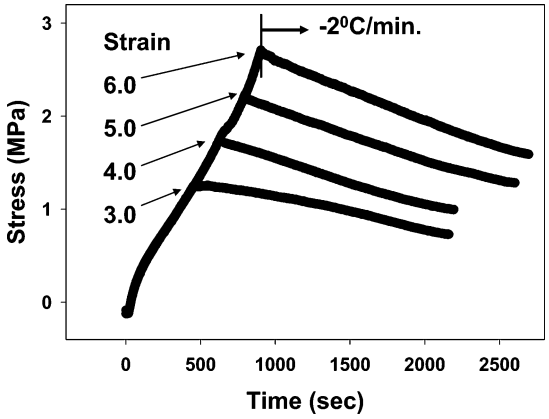

Figure 5. Stress changes during stretching at 30 °C and subsequent constrained cooling (at a rate of −2 °C/min) at strains 3.0, 4.0, 5.0, and 6.0.

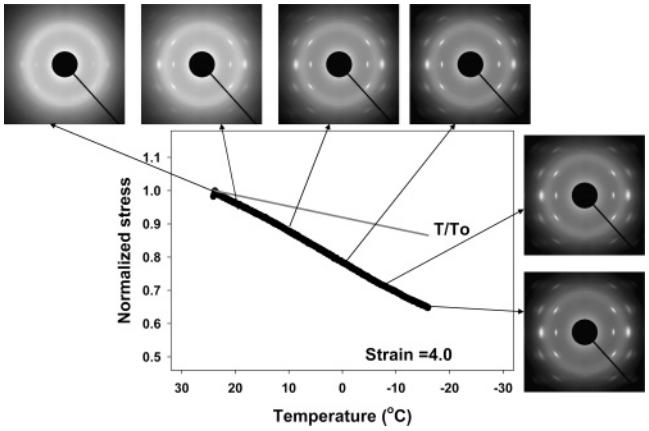

Figure 6. The normalized stress as a function of temperature at strain 4.0 during constrained cooling and selected 2D WAXD patterns. Each pattern was taken at the corresponding temperature indicated by the arrow. The straight line represents the expected value calculated by the entropy modulus prediction using eq 6.

3.0 was slightly different from the rest of the curves because strain-induced crystallization did not take place at 30 °C. Thus, the initially slow decrease in stress at strain 3.0 could be attributed to the entropy decrease at temperatures between 5 and 30 °C.

On the basis of the conventional concept, the decrease in temperature should cause thermal contraction, which would increase the stress. However, the above result shows an opposite trend for the stress change, indicating that the role of thermal contraction was minor or even negligible. One possible reason to explain the stress decrease is the reduction of entropy modulus due to the decrease in temperature. It is well known that vulcanized rubber is a material that exhibits entropy modulus.[3,5] Typically, rubber molecules between the network points can be expressed as Gaussian or non-Gaussian chains.[3,5] At small strains, one can assume that molecules are in the random coil state and behave as Gaussian chains. At large strains, molecules can be stretched and expressed as non-Gaussian chains. At strains above 3.0, our results have shown that the major fraction of amorphous molecules is in the random coiled state,[17,18,22,23] while some fraction of the chains is in the oriented (stretched) state and can be described by non-Gaussian chains. Therefore, we can first consider a scenario without strain-induced crystallization, i.e., the deformed system only contains amorphous phase with either Gaussian (random coiled) or non-Gaussian (stretched) chains.

The relationship between the force (F) and the extension ratio (α) for Gaussian and non-Gaussian chains can be expressed as follows[5]

$$F = NkTf(\alpha) \tag{3}$$

$$f(\alpha) = \alpha - 1/\alpha^2 \quad \text{(Gaussian)} \tag{4}$$

$$f(\alpha) = 1/3n^{1/2}\{\mathcal{L}^{-1}(\alpha/n^{1/2}) - \mathcal{L}^{-1}(1/\alpha^{1/2}n^{1/2})\} \quad \text{(non-Gaussian)} \tag{5}$$

where N is the total set of free chains, k is the Boltzmann coefficient, T is absolute temperature, n is the number of free segment units between network points, and $\mathcal{L}^{-1}$ is the inverse Langevin function. In the experiments, α is a constant during the temperature change, since we set the strain to be constant. To be precise, we set $\alpha = l/l_0 =$ strain + 1.0, since strain $= (l - l_0)/l_0$. Unless the total number of free chains or the network density is changed, the force should follow the equation at the constant strain condition following eq 3

$$F/F_0 = T/T_0 \tag{6}$$

where F, F_0, T, and T_0 represent the force and the absolute temperature at experimental temperature and at 30 °C, respectively. The equation is valid for both Gaussian and non-Gaussian chains.

The normalized stress change (the measured stress divided by the maximum stress) at strain 4.0 during the temperature reduction ramp (at a rate of −2 °C/min), the calculated stress change due to the reduction of entropy modules from the amorphous chains only (using eq 6) and selected 2D WAXD patterns at varying times (temperatures) are shown in Figure 6. The actual stress decrease was significantly larger than the calculated stress decrease due to the entropy modulus. The difference can be mainly attributed to the behavior of strain-induced crystallization, which can be explained as follows.

The relationship between the melting temperature (T_m) and deformation (uniaxial stretching) has been discussed by Yamamoto and White.[35] The melting point of an undeformed sample can be expressed as

$$T_{m,ud} = \Delta H_{ud}/\Delta S_{ud} \tag{7}$$

where ΔH_{ud} represents the heat of fusion and ΔS_{ud} represents the entropy of fusion in the undeformed state. When the sample is deformed, T_m increases as

$$T_{m,d} - T_{m,,ud} = (\Delta H_d/\Delta S_d) - (\Delta H_{ud}/\Delta S_{ud}) \tag{8}$$

where ΔH_d is the heat of fusion and ΔS_d is the entropy of fusion in the deformed state. If the heat of fusion is independent of deformation, then

$$1/T_{m,d} = (1/T_{m,ud}) - (\Delta S_{def}/\Delta H_{ud}) \tag{9}$$

where ΔS_{def} is the difference in entropy between the undeformed and the deformed states. It is thought that orientation, stretching, and partial ordering of polymer chains can all decrease the configurational entropy by an amount of ΔS_{def}. Since the melting temperature of

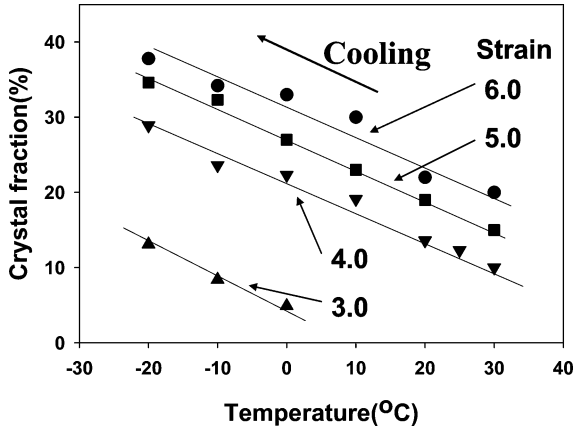

Figure 7. The change of crystal fraction during constrained cooling at strains 3.0, 4.0, 5.0, and 6.0.

strain-induced IR crystal is significantly higher than the experimental temperature (30 °C), which will be discussed later in this work, the stretched chains in the deformed sample are already in the supercooled state. The reduction of temperature thus generates a larger degree of supercooling, facilitating the crystallization process of these chains.[4,25−27,33] It is known that the increase in crystallization would decrease the bulk stress because the length of molecules in the stretching direction increases.[4,15,17,18,23−27]

The relationship between the strain-induced crystal fraction at different strains and temperatures during the cooling process (at a rate of −2 °C/min) is illustrated in Figure 7. It was seen that the crystal fraction increased almost linearly with decreasing temperature at all strains (3.0, 4.0, 5.0, and 6.0), where the slope of the relationship is about constant ($dX_c/dT \approx -0.5\%$ °C^{-1}). On the basis of extrapolation, at strain 3.0, the onset temperature of crystallization was about 5 °C.

In Figure 5, the decrease in stress during cooling can be attributed to two combined effects: (1) decrease in entropy force and (2) increase in strain-induced crystallization, both are caused by the changes of stretched amorphous chains. Although these two coupled effects cannot be easily separated, the effect of strain-induced crystallization appears to be the dominant one (as seen in Figure 6, where the entropy effect is only a minor factor). We illustrate the event of strain-induced crystallization and the possible changes during constrained cooling in Figure 8. Diagram A represents the development of strain-induced crystallites from stretched and oriented chains between the sulfur cross-linked bridges under uniaxial deformation. Upon crystallization, the average length of molecules along the stretching direction increases, resulting in a decrease of the overall force. During constrained cooling, the crystallization process is enhanced due to the increase in the degree of supercooling. However, the crystal growth may take place in two different directions, i.e., parallel (diagram B) and perpendicular (diagram C) to the stretching direction. The longitudinal crystal growth (diagram B) can result in extended chain conformation that will significantly alleviate the stress along the stretching direction, while the lateral growth would involve folded-chain conformation (diagram C) that may not decrease the stress. We thus speculate that the majority of the crystal growth during constrained cooling is along the stretching direction, as very large stress reduction has been seen. Although the schematic model elucidates the

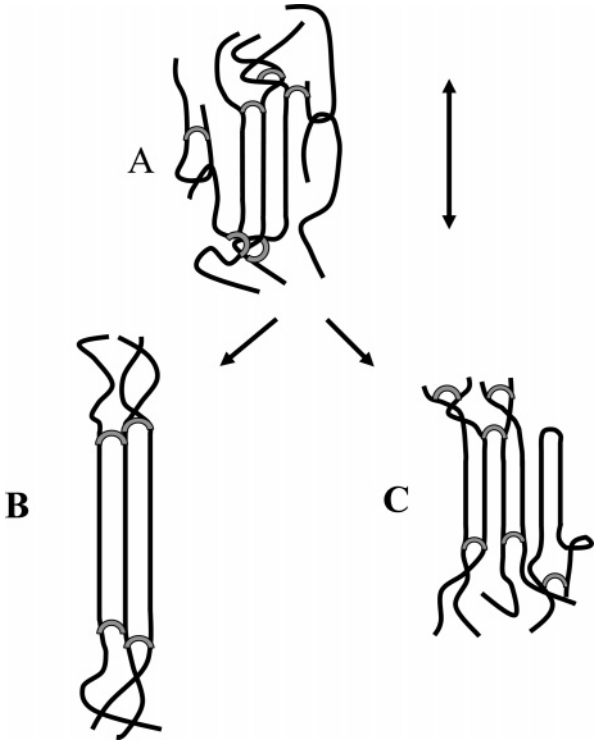

Figure 8. Schematic models of changes in strain-induced crystallites during constrained cooling: (A) initial strain-induced crystallites, (B) longitudinal crystal growth along the stretching direction, (C) lateral crystal growth perpendicular to the stretching direction.

possible mechanism to explain the stress decrease with increase of strain-induced crystallization, the relations between stress and strain may still follow eq 5.

We assumed that the deformed sample had a fiber symmetry and that the fiber direction coincided with the stretching direction.[16−19] Experimentally, this approximation had been confirmed in deformed rubber, as the WAXD patterns taken along the face-on and edge-on directions were found to be about the same (data not shown). Flory[3] also started his theory by assuming that the crystallite formed in deformed rubber had its fiber axis parallel to the direction of stretch. Although Flory acknowledged that the equilibrium crystallization decreases the tension in the stretched chains, his theory did not predict the thickness change in the crystallites. The theory elucidated that the increase in strain enhances T_m since the freedom of chain configuration is decreased by stretching; thus, it is more applicable to an equilibrium state. Our results are consistent with the basic idea of Flory's theory in spite that our experiments were carried out under nonequilibrium conditions.

The crystallite size of a rubber sample along the stretching direction (i.e., l_{002}) has been studied by Trabelsi et al.[20] using the tilting geometry to examine the undistorted intensity profile of the (002) diffraction under deformation. They observed some interesting relations between the crystal size (l_{002}) and strain: (1) the value of l_{002} in the sample deformed at −25 °C increased with the draw ratio λ, (2) l_{002} in the sample deformed at 23 °C did not show any dependency with λ, and (3) l_{002} in the sample first stretched at 90 °C and then quenched to 23 °C also increased with λ. Therefore, the crystal size dependency on strain clearly varies with the history of the deformation and thermal conditions.

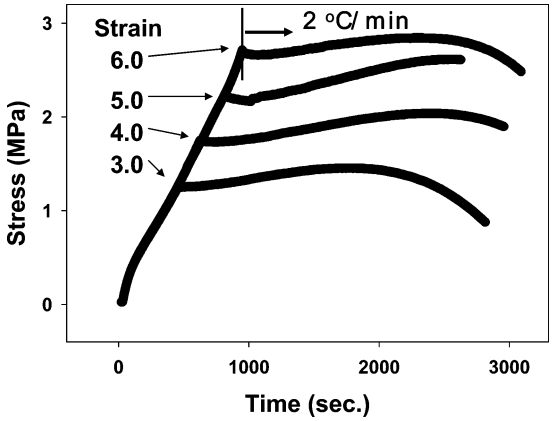

Figure 9. Stress changes during stretching at 30 °C and subsequent constrained heating (at a rate of 2 °C/min) at strains 3.0, 4.0, 5.0, and 6.0.

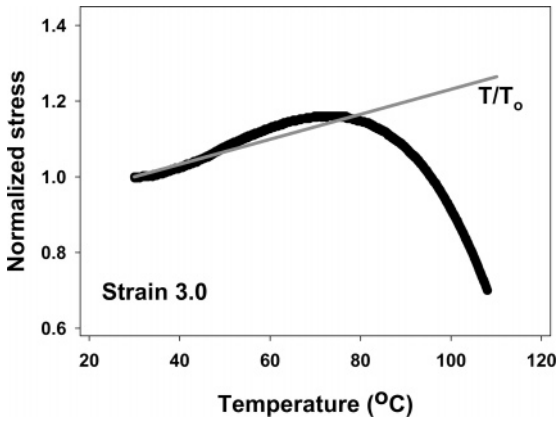

Figure 10. The normalized stress as a function of temperature during constrained heating at strain 3.0. The straight line represents the expected value calculated by the entropy modulus prediction using eq 6.

Their data are consistent with our results in this study, i.e., the crystal size increases with strain at low temperatures.

3. Stress Increase during Constrained Heating. After stretching to the desired strain at 30 °C, the sample was subjected to constrained heating at a rate of 2 °C/min. Results of the changes in stress are shown in Figure 9. It was found that the stress first increased then subsequently decreased with increasing temperature, resulting in a maximum value at certain temperatures that varied with strain. At strain 3.0, the stress reached its maximum at the lowest temperature, compared to those at larger strains. The initial inclines of the stress increase at strains 3.0, 4.0, and 5.0 were almost the same; however, the incline of the stress increase at strain 6.0 seemed to be much smaller than the rest.

The normalized stress value during constrained heating (at a rate of 2 °C/min and strain 3.0) is shown in Figure 10. Superimposed in Figure 10 is the expected stress response calculated from the concept of entropy modulus from stretched amorphous chains using eq 6. It was seen that the initial stress of vulcanized IR rubber practically followed the theory of rubber elasticity at strain 3.0, where no crystal diffraction was observed. The maximum stress was reached at around 75 °C. This suggests that the network density or the number of flexible chains between the network points starts to decrease at 75 °C under the constant strain of 3.0.

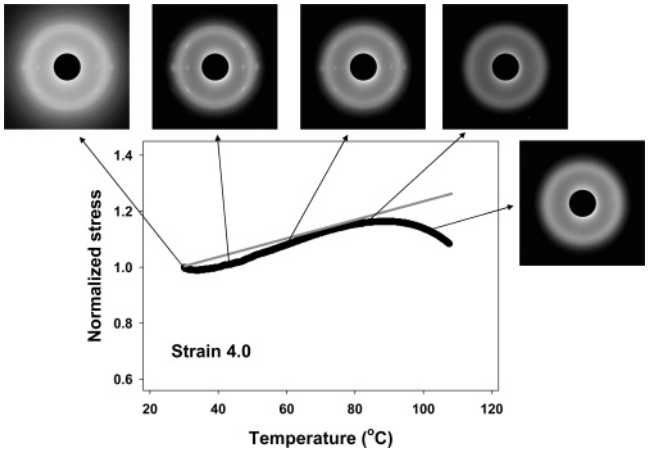

Figure 11. The normalized stress as a function of temperature during constrained heating at strain 4.0 and selected 2D WAXD patterns. Each pattern was taken at the corresponding temperature indicated by the arrow. The straight line represents the expected value calculated by the entropy modulus prediction using eq 6.

At strain 4.0, selected 2D WAXD patterns collected at different temperatures during constrained heating (at a rate of 2 °C/min) and the corresponding normalized stress are shown in Figure 11. Overall, the initial stress increase coincided with the entropy modulus prediction using eq 6, except for the small negative deviation observed at the low-temperature range (30−60 °C) that will be explained later. The stress exhibited a maximum value at around 88 °C, which was consistent with the disappearance of the crystalline diffraction patterns at about 85 °C (i.e., the melting temperature at strain 4.0). On the basis of the observation at this strain (4.0), where strain-induced crystallization occurs, the initial stress increase can be generally described by the theory of rubber elasticity (i.e., entropy modulus) over a large temperature range, and we hypothesize that the chemical network structure is preserved by the strain-induced crystalline network; the reduction of chemical network density and the melting of strain-induced crystallites appears to coincide at about 88 °C, which will be discussed by results from the next experiment.

Selected 2D WAXD patterns collected during constrained heating (at a rate of 2 °C/min) and corresponding normalized stress curves at strain 5.0 are shown in Figure 12. Even though the initial stress increase generally followed the trend predicted by the entropy modulus, the deviation between the experimental and theoretical values became significantly larger with the increasing strain. This phenomenon can be explained as follows. The additional stress decrease can be attributed to the enhancement of strain-induced crystallization with time, as shown in Figure 5. It was interesting to note that even the last crystalline diffraction pattern was seen at around 105 °C (data not shown), and the stress reached its maximum at 88 °C. This indicates that the thermal stability of the chemical network under strain is around 88 °C, above which the chemical network points (i.e., sulfur bridges) begin to degrade, even though the strain-induced crystalline network still remains (the maximum melting point at strain 5.0 is about 105 °C).

Selected 2D WAXD patterns collected during constrained heating (at a rate of 2 °C/min) and corresponding normalized stress curves at strain 6.0 are shown in Figure 13. It was seen that the initial stress increase

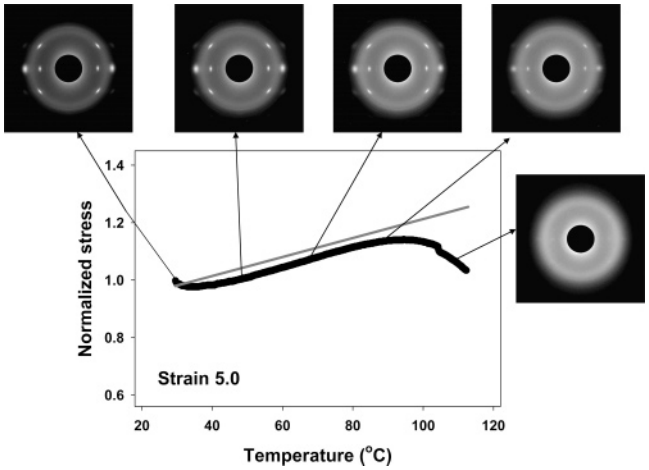

Figure 12. The normalized stress as a function of temperature during constrained heating at strain 5.0 and selected 2D WAXD patterns.

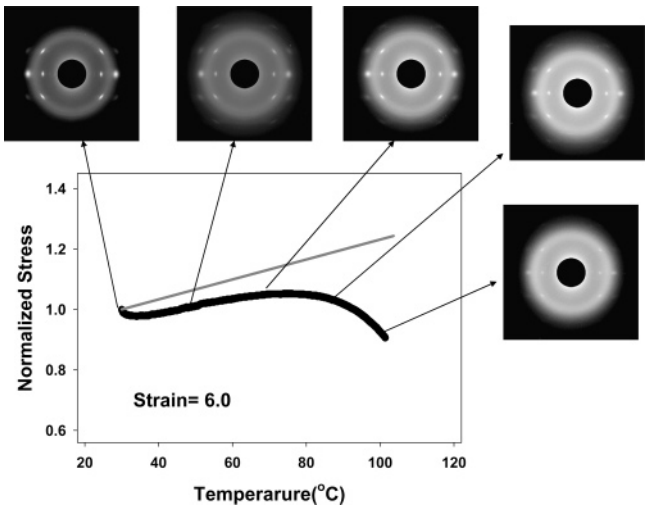

Figure 13. The normalized stress as a function of temperature during constrained heating at strain 6.0 and selected 2D WAXD patterns.

was notably reduced, which significantly deviated from the entropy prediction, although strain-induced crystallites remained stable above 100 °C. This observation can be attributed to at least two possible reasons. (1) As the stretched amorphous chains are highly constrained, they start to lose the freedom to alter their configurations. Therefore, the stress is no longer entropy modulus but more similar to energy modulus. However, as the observed crystal fraction is only around 20% (Figure 4) and based on our previous results indicating that the majority of amorphous molecules (more than 50%) are unoriented state even at high strains,[17,18,23,24] we believe that this reason is not the primary cause. (2) The sulfur bridges begin to transform their forms or even break at high strain (i.e., 6.0) with increasing temperature, which leads to a stress decrease. We believe this is the primary cause. It has been shown in the literature that the transformation of the sulfur bridges at high temperature is particularly prone to taking place at high strains and high stress conditions.[32,33]

The decrease of crystal fraction during constrained heating at a rate of 2 °C/min at different strains is shown in Figure 14. It was seen that the crystal fraction decreased almost linearly from 30 °C and disappeared

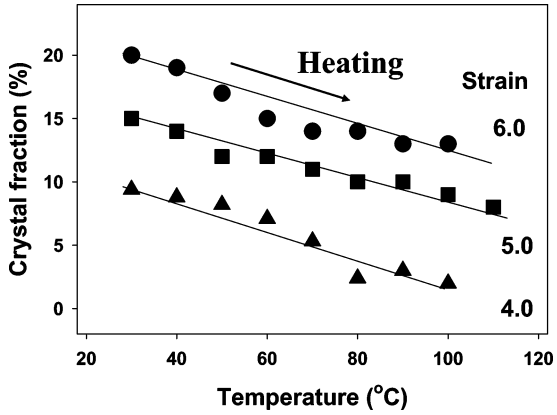

Figure 14. The change of crystal fraction during constrained heating at strains 3.0, 4.0, 5.0, and 6.0.

at around 100 °C for all three strains. Similar to the trend observed in Figure 7, the slope of the relationship between crystal fraction and temperature is also about constant ($dX_c/dT \approx -0.14\%$ °C^{-1}), that is, more than three times lower than the value observed in Figure 7. In Figure 14, it is clear that a large distribution of strain-induced crystallite size is produced under the chosen experimental conditions, and it is too broad to define a single characteristic T_m value (only the maximum value of T_m, i.e., $T_{m,max}$, can be defined). Recently, the values of $T_{m,max}$ have been reported for rubbers,[21,27,30] and they are significantly lower than the data reported here. The low $T_{m,max}$ values in the literature may be caused by the quenching procedures applied to the samples. For example, in these studies, the samples were all first stretched at room temperature[27,30] or 90 °C. [21] The strained samples were then placed in a cooling chamber at −6 °C for 10 days,[30] −20 °C for 24 h,[27] or −25 °C for 30 h.[21] The rapid quenching procedure increased the crystalline fraction, decreased the stress, and relaxed the amorphous molecules. As a result, the initially stretched amorphous molecules were substantially relaxed in these experiments. This situation is very different from the current work. In a way, our method of determining $T_{m,max}$ is relatively straightforward and can minimize the effect of additional thermal history.

Flory[3] suggested that strain-induced crystallites may function as additional network points of larger sizes, but our data does not support this argument since the melting of strain-induced crystallites does not decrease the stress significantly. Our results suggest that strain-induced crystallization reinforces the chemical network by building a scaffold around the existing chemical network points; it does not create new network points as in the form of a chemical network. In other words, we hypothesize that, under high strains, a hybrid network composed of chemical network points that are reinforced by strain-induced crystallites in the vicinity is developed.

Schematic models of the relationship between the strain-induced crystallites and sulfur bridges are shown in Figure 15. Diagram A indicates that, before deformation or below strain 3.0, the strain-induced crystallization does not occur and the rubber is composed of mainly amorphous molecules and network points (sulfur bridges). Diagram B indicates that, at strain around 3.7, strain-induced crystallization starts to develop, but only certain molecules between the sulfur bridges are crystallized. This process does not increase the chemical

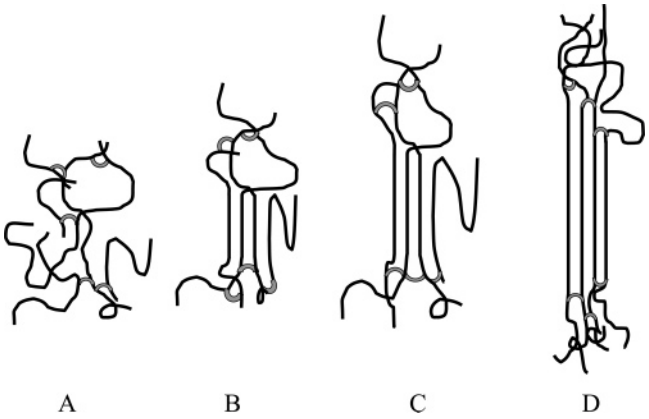

Figure 15. Schematic models of strain-induced crystallites at different strains: (A) the initial chemical network containing sulfur bridges, (B) at low strains, parts of flexible chains are crystallized between the sulfur bridges, (C) at intermediate strains, more chains between sulfur bridges become crystallized, and (D) under high strains, all chains between the sulfur bridges are crystallized, resulting in a new effective crystalline network structure.

network density or the number of flexible chains between chemical network points. Diagram C indicates that, at strains 4.0 and 5.0, strain-induced crystallites develop further along the stretching direction, but only parts of the molecules between the network points are crystallized, where the rest of the molecules still possess freedom to alter their configurations.[4,17,23−25,27] With the increase of strain-induced crystallization (i.e., through the growth of extended chain crystal), a new reinforced network is developed along the stretching direction. This mechanism can increase the elongation at break in rubber. Diagram D indicates that, at strain 6.0, the majority of molecules between the chemical network points are crystallized. The strain-induced crystallites are connected by some stretched chains that are noncrystalline, which forms the crystalline network that is closely coupled with the chemical network. The hybrid network structures are strong enough to endure high strains and high stress values, but the chemical network may break down at high temperatures (ca. 88 °C).

4. Excess Strain-Induced Crystallites during Constrained Heating. The nature of strain-induced crystallization was further explored by the following experiment. After stretching to strain 6.0, the sample was subsequently retracted to strain 4.0 and subjected to constrained heating measurements. Selected WAXD patterns, the stress responses during extension (to strain 6.0) and then retraction (to strain 4.0), and the normalized stress during constrained heating, are illustrated in Figure 16. It was found that the stress during retraction was significantly lower than the stress during stretching. It was also found that the crystal fraction during retraction was larger than the one during stretching (as seen in the WAXD images at strain 4.0 in Figure 16). Both hystereses have been reported before.[16−19,23−25] During constrained heating, the initial sample at strain 4.0, after being stretched to strain 6.0, possessed a higher degree of strain-induced crystallites than that without being first stretched to strain 6.0 (Figure 11). The corresponding stress change upon heating exhibited an increase in temperature,[14,15] substantially larger than the expected values from the entropy consideration using eq 6. This behavior is due to the melting of the excess strain-induced crystallites, which subsequently increased the number of flexible chains and increased the stress.

The occurrence of strain-induced crystallization has two coupled effects on stress: the creation of a new network structure that increases the stress and the "freezing" of flexible amorphous chains that decreases the stress. In the case of the excess crystallites determined upon retraction, our results are consistent with the "melting" of frozen flexible chains, which increases the stress. The excess crystallites represent the crystallites that were induced at strain 6.0 but remained after retraction to strain 4.0. Schematic diagrams of the mechanism for excess strain-induced crystallites during constrained heating are shown in Figure 17. Diagram A indicates that, at strain 4.0, strain-induced crystallization occurs in the part of the amorphous chains between the network points (sulfur bridges). Diagram B indicates that, at strain 6.0, all chains between the network points are crystallized. Diagram C indicates

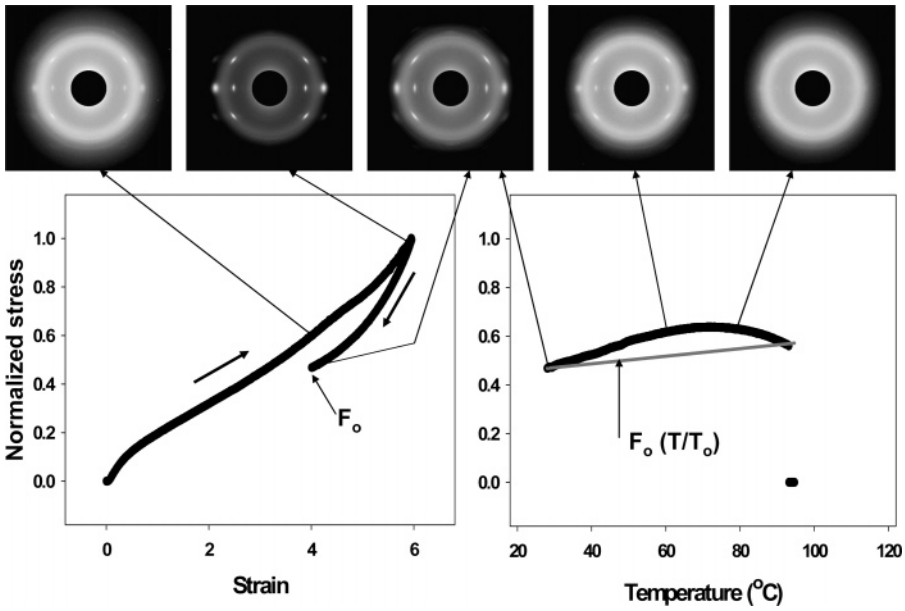

Figure 16. Stress−strain curves during extension to strain 6.0 and then retraction to strain 4.0 at 30 °C (left); corresponding stress changes during subsequent constrained heating (right). Selected 2D WAXD patterns were collected at varying strain conditions and temperatures, which are indicated by the arrows.

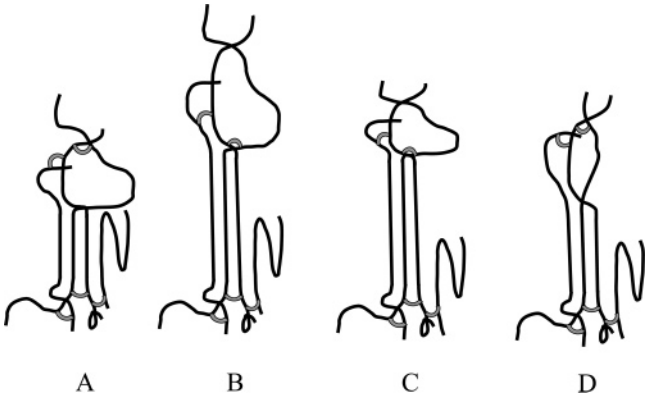

Figure 17. Schematic diagrams of excess strain-induced crystallites during constrained heating: (A) at strain 4.0, strain-induced crystallization occurs between the cross-linking points (sulfur bridges), (B) at strain 6.0, the majority of chains are crystallized between the sulfur bridges, (C) at strain 4.0 upon retraction from strain 6.0, excess strain-induced crystallites remain, and (D) during constrained heating at strain 4.0, excess crystallites melt and the stress increases.

that, at strain 4.0 after retracting from strain 6.0, the crystallites between the network points remain as excess crystallites. Diagram D indicates that, at strain 4.0 during constrained heating, the strain-induced crystallites start to melt and increase the stress.

Conclusions

The nature of strain-induced crystallization in vulcanized IR rubber was examined by thermomechanical methods in combination with in situ synchrotron WAXD. Results from constrained cooling and heating indicated that the hybrid structures of the chemical network (containing sulfur bridges as network points) and the strain-induced crystalline network dictate the mechanical properties, where both networks change continuously under different thermomechanical conditions. Other important summary remarks for this work are as follows.

1. Strain-induced crystallization generally decreases the stress and increases the bulk elongation due to the increase in (crystalline) chain length along the stretching direction. The elongation at break ratio of vulcanized rubber thus depends on the ability of strain-induced crystallization under deformation.

2. The melting of strain-induced crystallites increases the stress due to the decrease in average chain length between the crystalline network points.

3. The chemical network points (sulfur bridges) can be significantly reinforced by strain-induced crystallites. These chemical network points can be degraded under high strain conditions at high temperatures (above ca. 88 °C). The dynamic response of the hybrid network structures containing strain-induced crystalline and chemical network points is responsible for the tensile strength of vulcanized rubber.

Acknowledgment. The financial support of the U.S. team was provided by the National Science Foundation (DMR-0405432) and Yokohama Rubber. The Japanese team was supported by a Grant-in-Aid for Scientific Research (B)(2), No. 15404011 from the Japan Society for the Promotion of Science.

References and Notes

(1) Erman, B.; Mark, J. E. *Structures and properties of rubber like networks*; Oxford University Press: 1997.
(2) Alfrey, T.; Mark, J. E. *J. Chem. Phys.* **1942**, *46*, 11.
(3) Flory P. J. *J. Chem. Phys.* **1947**, *15*, 397.
(4) Flory, P. J. *Principles of Polymer Chemistry*, Cornell University Press: Ithaca, NY, 1953.
(5) Treloar, R. G. *The Physics of Rubber Elasticity*, 3rd ed.; Oxford University Press: Oxford, 1975.
(6) Treloar, R. G. *Trans. Faraday. Soc*. **1947**, *43*, 277; Treloar, R. G. *Trans. Faraday. Soc*. **1947**, *43*, 284.
(7) Guth, E.; James, H. M. *Ind. Eng. Chem.* **1941**, *33*, 621.
(8) Boyce, C.; Arruda, E. M. *Rubber Chem. Technol.* **2000**, *73*, 504.
(9) Gehman, S. D.; Field, J. E. *J. Appl. Phys.* **1939**, *10*, 564.
(10) Bunn, C. W. *Proc. R. Soc., A* **1942**, *180*, 40.
(11) Luch, D.; Yeh, G. S. Y. *J. Macromol. Sci.* **1973**, *B7* (1), 121.
(12) Shimomura, Y.; White, J. L. *J. Appl. Polym. Sci.* **1982**, *27*, 3553.
(13) Mitchell, G. R. *Polymer* **1984**, *25*, 1562.
(14) Toki, S.; Fujimaki, T.; Okuyama, M. *International Seminar on Elastomers*; 1985 Proceedings; p 84.
(15) Toki, S.; Fujimaki, T.; Okuyama, M. *Polymer* **2000**, *41*, 5423.
(16) Murakami, S.; Senoo, K.; Toki, S.; Kohjiya, S. *Polymer* **2002**, *43*, 2117.
(17) Toki, S.; Sics, I.; Ran, S.; Liu, L.; Hsiao B. S.; Murakami S.; Senoo, K.; Kohjiya, S. *Macromolecules* **2002**, *35*, 6578.
(18) Toki, S.; Sics, I.; Ran, S.; Liu, L.; Hsiao, B. S. *Polymer* **2003**, *44*, 6003.
(19) Toki, S.; Hsiao, B. S. *Macromolecules* **2003**, *36*, 5915.
(20) Trabelsi, S.; Alobouy, P. A.; Rault, J. *Macromolecules* **2003**, *36*, 7624.
(21) Trabelsi, S.; Alobouy, P. A.; Rault, J. *Rubber Chem. Technol.* **2004**, *77*, 304.
(22) Tosaka, M.; Murakami, S.; Poompradub, S.; Kohjiya, S.; Ikeda, Y.; Toki, S.; Sics, I.; Hsiao, B. S. *Macromolecules* **2004**, *37*, 3299.
(23) Toki, S.; Sics, I.; Hsiao, B. S.; Murakami, S.; Tosaka, M.; Poompradub, S.; Kohjiya, S.; Ikeda, Y. *J. Polym. Sci., Part B: Polym. Phys.* **2004**, *42*, 956.
(24) Toki, S.; Sics, I.; Hsiao, B. S.; Murakami, S.; Tosaka, M.; Poompradub, S.; Kohjiya, S.; Ikeda, Y. *Rubber Chem. Technol.* **2004**, *77*, 317.
(25) Toki, S.; Sics, I.; Hsiao, B. S.; Murakami, S.; Tosaka, M.; Poompradub, S.; Kohjiya, S.; Ikeda, Y. *ACS Rubber Div. Preprint* **2004**, paper#20.
(26) Miyamoto, Y.; Yamano, H.; Sekimoto, K. *Phys. Rev. Lett.* **2002**, *88*, 225504.
(27) Miyamoto, Y.; Yamano, H.; Sekimoto, K. *Macromolecules* **2003**, *36*, 6462.
(28) Gent, A. N. *Trans. Faraday Soc.* **1954**, *50*, 521.
(29) Gent, A. N.; Kawahara, S.; Zhao, J. *Rubber. Chem. Technol.* **1998**, *71*, 668.
(30) Gent, A. N.; Zhang, J. *J. Polym. Sci., Part B: Polym. Phys.* **2001**, *39*, 811.
(31) Mitchell, J. C.; Meier, D. J. *J. Polym. Sci., Part A: Polym. Chem.* **1968**, *6*, 1689.
(32) Fraser, R. D.; Macrae, T. P.; Miller, A.; Rowlands, R. J. *J. Appl. Crystallogr.* **1976**, *9*, 81.
(33) Nakauchi, H. *J. Soc. Rubber Ind. Jpn.* **1987**, *60*, 273.
(34) Nakauchi, H. *J. Soc. Rubber Ind. Jpn.* **2002**, *75*, 73.
(35) Yamamoto, M.; White, J. L. *J. Polym. Sci.* **1971**, *A-2 9*, 1399.

MA050465F